

Static-, Dynamic-, and Mixed-Eccentricity Fault Diagnoses in Permanent-Magnet Synchronous Motors

Bashir Mahdi Ebrahimi, Jawad Faiz, *Senior Member, IEEE*, and Mehrrsan Javan Roshtkhari

Abstract—Mixed-eccentricity (ME) fault diagnosis has not been so far documented for permanent-magnet (PM) synchronous motors (PMSMs). This paper investigates how the static eccentricity (SE), dynamic eccentricity (DE), and ME in three-phase PMSMs can be detected. A novel index for noninvasive diagnosis of these eccentricities is introduced for a faulty PMSM. The nominated index is the amplitude of sideband components with a particular frequency pattern which is extracted from the spectrum of stator current. Using this index makes it possible to determine the occurrence, as well as the type and percentage, of eccentricity precisely. Meanwhile, the current spectrum of the faulty PMSM during a large span is inspected, and the ability of the proposed index is exhibited to detect eccentricity in faulty PMSMs with different loads. A novel theoretical scrutiny based on a magnetic field analysis is presented to prove the introduced index and generalize the illustrated fault recognition method. To show the merit of this index in the eccentricity detection and estimation of its severity, first, the correlation between the index and the SE and DE degrees is determined. Then, the type of the eccentricity is determined by a k -nearest neighbor classifier. At the next step, a three-layer artificial neural network is employed to estimate the eccentricity degree and its type. After all, a white Gaussian noise is added to the simulated current, and the robustness of the proposed index is analyzed with respect to the noise variance. In this paper, the PMSM under magnetic fault (demagnetization) and electrical faults (short and open circuits) is modeled, and the current spectrum of the faulty PMSM under demagnetization, short circuit, and open circuit faults is analyzed. It is demonstrated that the proposed index, due to eccentricity fault, is not generated in the current spectrum due to magnetic and electrical faults. Indeed, it is exposed that the introduced index is only created due to eccentricity fault and it is not sensitive to other faults. To model the PMSM eccentricities, a time-stepping finite-element method, which takes into account all geometrical and physical characteristics of the machine components, nonuniform permeance of the air gap, and nonuniform characteristics of the PM material, is employed. This model facilitates the access to the demanded signals in order to have accurate processing. A comparison of simulation and experimental results validate the proposed index.

Index Terms—Amplitude of sideband components (ASBC), artificial neural network (ANN), dynamic eccentricity (DE) and mixed eccentricity (ME), fault diagnosis, Gaussian noise, pattern recognition, permanent-magnet (PM) synchronous motor (PMSM), static, time-stepping finite-element (FE) method (FEM) (TSFEM).

Manuscript received November 30, 2008; revised July 30, 2009. First published August 28, 2009; current version published October 9, 2009.

The authors are with the Center of Excellence on Applied Electromagnetics Systems, School of Electrical and Computer Engineering, University of Tehran, Tehran 1439957131, Iran (e-mail: ebrahimibm@ut.ac.ir; jfaiz@ut.ac.ir; m.javan@ece.ut.ac.ir).

Color versions of one or more of the figures in this paper are available online at <http://ieeexplore.ieee.org>.

Digital Object Identifier 10.1109/TIE.2009.2029577

I. INTRODUCTION

PERMANENT-MAGNET (PM) synchronous motors (PMSMs) are widely used in industry due to their higher torque, higher output to volume ratio, and better dynamic performance compared to the motors with electromagnetic excitation, simple construction, and easy maintenance. In order to increase PMSM performance, raise their lifetime, and lower their high costs, fault prediction in PMSMs is necessary. According to Fig. 1, faults in PMSMs are classified into three parts: electrical, magnetic, and mechanical faults. Due to having access to the stator of the motor, the detection of electrical fault in faulty PM is much easier in magnetic or mechanical faults. In [1], wavelet packet (WP) transform has been employed for feature extraction. The features are energy at the four nodes of the transformed current with $db3$ wavelet basis function. Then, the occurrence of fault is detected using artificial neural networks (ANNs) in both line- and inverter-fed interior PMSMs. The studied faults are three common electrical faults, which are a momentarily opening of one phase between the motor and the inverter, and line-to-ground and line-to-line short circuits in the stator windings. As the features are energy at various nodes of WP decomposition of stator current, other faults (e.g., eccentricity), which have an effect on the rms value of the current, may be classified as electrical faults. Thus, other indices must be used, which are exactly related to the fault. In [2], the electrical faults (short circuit and breaking of contact) and one mechanical fault (worn gears, which are simulated by removing portions of gear teeth) have been detected. Features are extracted from four time–frequency analysis methods of stator current, which are short-time Fourier transform, undecimated wavelet analysis, and the Wigner and Choi-Williams distributions of the field-oriented currents in PM ac drives. After applying the multiple-class discriminated analysis for feature dimension reduction, the classification of fault types is performed by using k -means and linear discriminated classifiers. An analytical model that predicts the short-circuit current in a fault-tolerant PM machine under partial-turn short-circuit fault conditions, which can be used for model-based short-circuit fault detection systems in PM machines, has been described in [3]. This model quantifies the variation of slot-leakage flux as a function of the relative position of partially short-circuited turns. Electrical fault detection by this model may have accurate results, but it needs preknowledge of the motor structure.

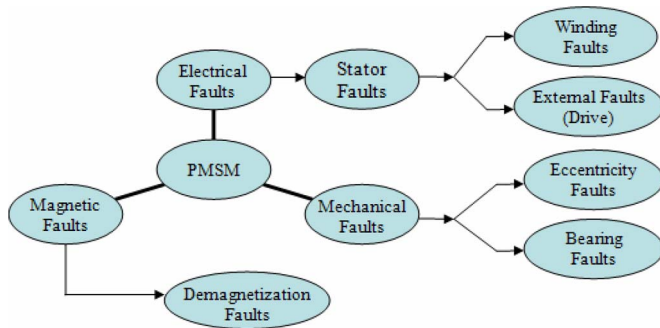


Fig. 1. Block diagram of PMSM fault categories.

Mechanical faults involve bearing and eccentricity faults. Eccentricity faults consist of static eccentricity (SE), dynamic eccentricity (DE), and mixed eccentricity (ME). They occur due to manufacturing imprecision such as unbalanced mass, shaft bow, and bearing tolerance. Eccentricity may cause magnetic and dynamic problems with additional vibrations, noises, and torque pulsations. Although the eccentricity faults in induction motors are extensively investigated [4]–[7], there are a few publications on PMSMs with eccentricity. In [8], an analytical method, based on a 2-D magnetic field theory in polar coordinates, neglecting slotting effect, is used to analyze eccentricity faults. It is noticeable that ignoring stator slots has many effects on the performance calculation of the motor. Flux density distribution along the surface of the stator has been calculated by a perturbation method. In [9], an analytical method has been presented to predict the instantaneous magnetic field distribution in the air gap of the PMSM with SE and DE faults. The governing equations have been solved, and associated boundary conditions have been imposed by the perturbation method. The predicted result is then verified by the corresponding finite-element (FE) method (FEM) results. Since calculating the magnetic field is an invasive fault diagnosis method, the use of magnetic flux density for fault diagnosis is not recommended. In [10], a magnetic force acting on the iron surface of interior PM (IPM) and surface PM (SPM) motors has been determined using the Maxwell stress tensor. It has been presented that SE fault can increase magnetic flux density, radial force density, unbalanced magnetic pull (UMP), and harmonic components in radial force density. However, invasive fault diagnosis by some signals, such as magnetic field density, radial force, and UMP, is unimpressive. Meanwhile, the effects of DE and the discrimination of SE and DE have not been shown. In [11], unbalanced force, cogging torque, back electromotive force (EMF), local traction, torque ripples, and phase current have been calculated analytically in eccentric PM motor. In the case of eccentricity, the distortion of back EMF and phase current increase the torque ripples and, in the worst case, increase both the unbalanced force and cogging torque of the PMSM. In addition, it is noticeable that the amplitude of phase current is not a proper index for fault diagnosis because it changes with load and other existing faults. Therefore, the diagnosis of the eccentricity fault will be very difficult if only the amplitude of the current is used. In [12] and [13], the cogging torque in PM brushless motor

has been calculated using the air-gap magnetic field energy and classical equation of the air-gap magnetic flux density distribution. In [14], the characteristics of the unbalanced magnetic forces and cogging torque have been examined for various slot angles using FEM and shown that they cannot be minimized simultaneously by adjusting the slot angle. To reduce the magnetic force harmonics, the slot angle needs to be as small as possible. To minimize the cogging torque, the slot angle must be close to 18° . Meanwhile, it has been shown that unbalanced magnetic forces have dominant effects on the magnetically induced vibration of spindle motor, and the proper trend of a brushless dc motor design minimizes the unbalanced magnetic forces when both minimum cogging torque and reduced magnetic forces are not achievable simultaneously. In [15], the demagnetization states of PMs during fault conditions in a PMSM are analyzed, and the ability of the motor to sustain the designed rated outputs after the fault has been analyzed is characterized. Meanwhile, torque, line voltage, and current have been calculated for the analysis of PMSM with a short-circuit fault. In [16], the performance of a multiphase doubly salient PM motor has been analyzed to predict the effects of the eccentricity fault on one half of the rotor and elliptical rotor. It has been shown that the magnitude of the harmonic components in the developed torque is increased. In [17], SE and DE, misalignment, and broken magnet in PMSM have been diagnosed using the spectrum analysis of the current experimentally. The amplitude of harmonic components at 25 Hz has been introduced as an index for fault diagnosis. It is noted that the amplitude of the aforementioned harmonic components is not a suitable index for fault diagnosis, because it can be influenced by some parameters such as load. In [18], the performances of SPM and IPM with SE fault have been compared. It has been shown that the air-gap flux density and induced EMF of the SPM motors are less sensitive to rotor eccentricity than that of IPM motors.

In this paper, PMSM with SE, DE, and ME is modeled using time-stepping FEM (TSFEM). In this modeling, the geometrical and physical characteristics of different parts of PMSM, nonuniform permeance of air gap due to stator slots, nonlinear characteristics of PM, and stator and rotor cores are considered. Then, stator current, calculated using TSFEM, is chosen as a proper signal for processing and noninvasive fault diagnosis. Fast Fourier transform (FFT) is then used to process the stator current. Therefore, a novel frequency pattern for SE, DE, and ME is introduced, and the amplitude of sideband components (ASBC) at frequencies extracted from the frequency pattern is used to diagnose the different eccentricities of fault. Meanwhile, the ability of the proposed index for eccentricity fault detection is examined in terms of their relation to SE, DE, and capability for identifying the eccentricity type. Moreover, their robustness is analyzed with respect to additive measurement noise variance. Following the determination of correlation coefficient between indices and SE and DE degrees, the type of eccentricities is determined using a k -nearest neighbor (NN) classifier. After all, a three-layer ANN is employed to estimate the eccentricity degree of current profile based on the eccentricity type.

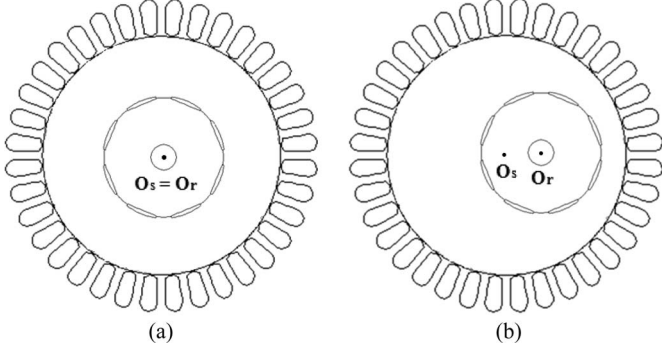


Fig. 2. Cross section of PMSM. (a) Healthy. (b) SE.

TABLE I
SPECIFICATIONS OF THE PROPOSED THREE-PHASE PMSM

Number of poles	8
Effective length of stator core (m)	0.0475
Stator inner diameter (m)	0.2472
Air-gap length (m)	0.0008
Height of stator yoke (m)	0.0504
Height of stator slot (m)	0.0387
Number of turns per phase	528
Number of stator slots	36
Remanent flux density of PM (T)	1.06
Rated voltage, V	200
Rated frequency, Hz,	50
Rated power (W)	3500

II. TIME-STEPPING FE MODELING

Almost all the reliable fault diagnosis methods are based on detailed real parameters and practical conditions. A proper and precise modeling is the first step in the fault diagnosis process. Precise modeling methods based on the magnetic field computation take the detailed machine structure into account in order to obtain highly accurate results. Here, a PMSM with SE, DE, and ME is modeled using TSFEM. Fig. 2 shows the cross sections of the healthy and faulty PMSM with SE. The specifications of the proposed three-phase PMSM have been summarized in Table I. In the modeling, the geometrical complexities of all parts of the motor, including stator, rotor, and shaft, are included. Moreover, the spatial distribution of the stator windings, nonuniform air gap, the physical conditions of stator conductors, rotor, shaft and air gap, and the nonlinearity of core materials are taken into account. A three-phase sinusoidal voltage applied to the terminals of the motor is the input. The transient equations of the external circuit and circuit elements are combined with the magnetic field equations. In addition, motion equations are combined with the magnetic field equations in the FEM in which the motion equations are combined with these equations. The solution of the set of equations gives the stator phase current as the principal variable. In 2-D Cartesian system, the electromagnetic equation analyzed by FEM is given as follows:

$$\frac{\partial}{\partial x} \frac{1}{\mu} \left(\frac{\partial A}{\partial x} \right) + \frac{\partial}{\partial y} \frac{1}{\mu} \left(\frac{\partial A}{\partial y} \right) = J_0 + J_e + J_\nu \quad (1)$$

where A is the z -component of magnetic vector potential, and μ is the magnetic permeability. J_0 is the current density related to the applied voltage, J_e is the current density related to the time

variations of the magnetic flux, and J_ν is the current density related to the motional voltage. Therefore, (1) is rewritten as follows:

$$\frac{\partial}{\partial x} \frac{1}{\mu} \left(\frac{\partial A}{\partial x} \right) + \frac{\partial}{\partial y} \frac{1}{\mu} \left(\frac{\partial A}{\partial y} \right) = -\sigma \frac{V_s}{\ell} + \sigma \frac{\partial A}{\partial t} + \sigma \nu \times \nabla \times A \quad (2)$$

where σ is the electrical conductivity, ℓ is the motor length along the z -axis, V_s is the applied voltage, and ν is the speed of the conductor against magnetic flux density. By the application of a reference frame that is assumed fixed with respect to the proposed element, ν is equal to zero, and the propagation equation is simplified as follows:

$$\frac{\partial}{\partial x} \frac{1}{\mu} \left(\frac{\partial A}{\partial x} \right) + \frac{\partial}{\partial y} \frac{1}{\mu} \left(\frac{\partial A}{\partial y} \right) = -\sigma \frac{V_s}{\ell} + \sigma \frac{\partial A}{\partial t} \quad (3)$$

The circuit equation of the magnetic coil is given as follows:

$$V_s = R_s i + N \frac{d\varphi}{dt} \quad (4)$$

where R_s is the coil resistance, i is the current in the coil, N is the number of turns, and φ is the coil flux linkage. The time difference terms in (3) and (4) are calculated by the backward difference method as follows:

$$\frac{dA^{t+\Delta t}}{dt} = \frac{A^{t+\Delta t} - A^t}{\Delta t} \quad \frac{d\varphi^{t+\Delta t}}{dt} = \frac{\varphi^{t+\Delta t} - \varphi^t}{\Delta t} \quad (5)$$

The initial values of A and φ are set to zero. By coupling (3), and (4), the TSFEM is used to obtain the magnetic vector potential and stator current. The nonlinear equation, which can relate the FE equations expressing the electromagnetic fields of the machine with the circuit equations, is as follows:

$$[C][A \quad \Delta V \quad i]^T + [D] \left[\frac{\partial A}{\partial t} \quad \frac{\partial \Delta V}{\partial t} \quad \frac{\partial i}{\partial t} \right]^T = [Q] \quad (6)$$

The solution of (6) gives $[A]$ and $[i]$. $[C]$ and $[D]$ are the coefficients matrices, and $[Q]$ is the vector related to the input voltage. The distribution of the magnetic flux density is determined by A as follows:

$$\vec{B} = \nabla \times \vec{A} \quad (7)$$

The magnetic field distribution of air gap contains all information about the stator and rotor positions and mechanical parts of the motor. Thus, continuous monitoring of the air-gap magnetic field makes it possible to diagnose all faults in electrical motors [19]. Air-gap magnetic field has the following distribution:

$$B_{\text{normal}} = \sum_{n=1,3,5,\dots} B_n \sin(n\omega t) + \sum_{n=2,4,6,\dots} B_n \cos(m\omega t) \quad (8)$$

In (8), the odd harmonics form the fundamental waves of the air-gap flux density, and the even harmonics form the magnetomotive force (MMF) ripples. Fig. 3 shows the magnetic flux density distribution of the healthy and faulty motor under SE and DE. As shown in Fig. 3, eccentricity causes asymmetrical

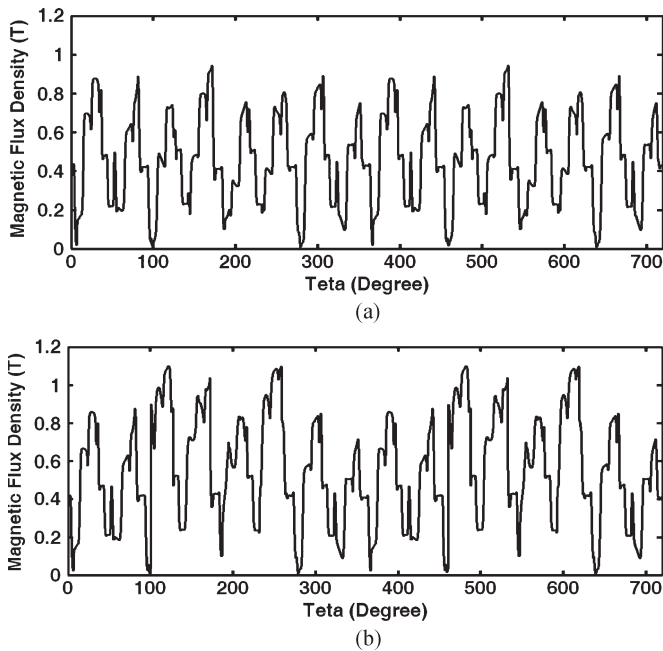


Fig. 3. Magnetic flux density in full-load PMSM air gap. (a) Healthy. (b) With 30% DE.

magnetic flux density distribution. When eccentricity occurs, the air-gap field consisting of the fundamental component, such as stator and rotor MMF harmonics and stator and rotor slot permeances, will have additional harmonic components due to the fault. Meanwhile, the fundamental harmonic degree and ripples vary with the type and eccentricity degree. Harmonic components generated in the magnetic flux density of air gap due to eccentricity are seen in stator current. The distortion of magnetic flux density in motor air gap increases ripples and generates harmonic components in torque and speed profiles. Thus, faulty motor inductances are distorted, and the mentioned harmonics are seen in inductance profiles. Consequently, stator currents are distorted, and special harmonic components are generated in stator current profiles, which can be utilized to recognize eccentricity fault. Therefore, the spectrum analysis of stator current in faulty motor can be used as an appropriate attitude for noninvasive eccentricity fault detection.

III. EXPERIMENTAL SETUP

A general plan of the experimental setup is shown in Fig. 4. This system can be used to sample two line currents I_a and I_b , two line voltages V_{ab} and V_{bc} , and a speed signal (by an angular speed sensor). The motor windings are Δ connected, and the third line current (I_c) and line voltage (V_{ca}) can be easily estimated from the sampled currents and voltages, respectively. The main parts of the experimental setup with numbers shown in the figure are as follows:

- 1) a three-phase 3.5-kW PMSM with specifications given in Table I;
- 2) a dc generator coupled to the PMSM to provide load variation;
- 3) a Tacho generator coupled to the shaft of the generator as angular speed sensor to measure and record the time variation of the speed;

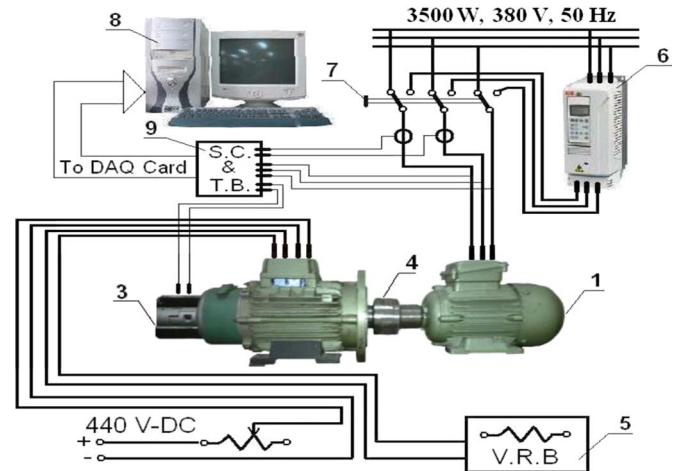


Fig. 4. Experimental setup.

- 4) mechanical coupling between PMSM and dc generator;
- 5) a variable resistor bank as a variable load of the generator; the load of generator and, consequently, PMSM can be adjusted by varying this resistance and/or regulating the excitation current of generator by a relevant variable resistor;
- 6) a PMSM drive from ABB Company with rating values corresponding to the rated values of the motor;
- 7) a three-phase changeover switch for exchanging the motor connection from the main to the drive output and vice versa. It is noted that the three-phase supplies of the laboratory contain on and off switches and protection devices, which are shown in Fig. 4;
- 8) a PC equipped with a data acquisition (DAQ) card of type PCI-1710HG from Advantech on its PCI bus for sampling the electrical data at certain adjustable frequency and storing them in the memory [23];
- 9) signal conditioning and terminal box: Since card PCI-1710HG accepts only voltage-type signals with a maximum amplitude of ± 10 V at its analog inputs, the type and range of the proposed signals for sampling must be prepared before connecting to this card. The voltage-type signals (two line voltages of motor and speed signal from tacho-generator output) can be easily prepared using a resistive voltage divider [23]. To enhance the accuracy, high-precision class resistances can be used. To prepare the current signals, isolation from power circuit is necessary first. In Fig. 4 scheme, current transformers with a precision class of 0.1 play this role. Then, current shunts are used to convert secondary side currents into voltages. To facilitate the connection of signals to DAQ card, a special terminal box-type Advantech-PCLD-8710 has been used. The signals have been easily connected to this terminal box by screw connectors. All signals have been then transmitted to DAQ card using a special shielded cable of type Advantech-PCL-10168.

ME in PMSMs is created by a ball bearing, where its inner diameter, enclosing the shaft, is slightly larger than that of the shaft and its outer diameter placed in a specific room on the motor bung is smaller than the mentioned inner diameter

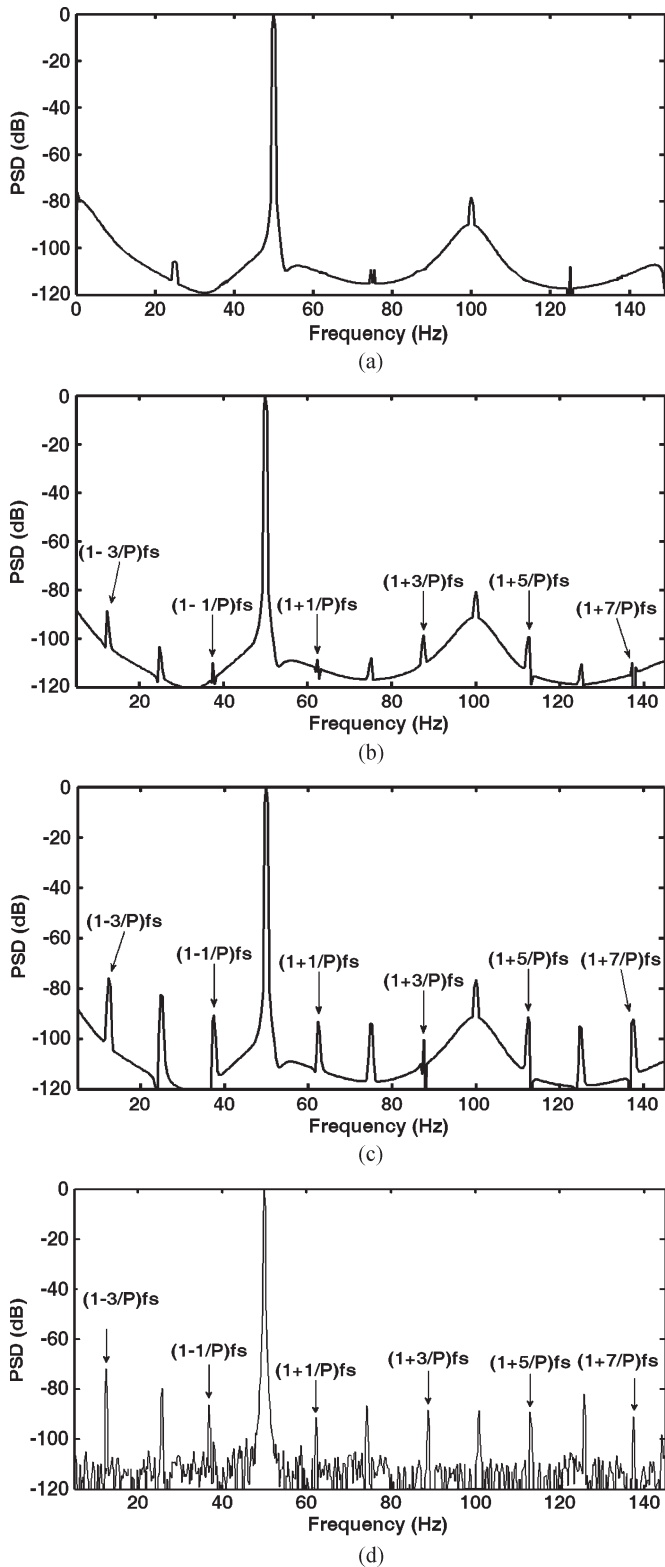


Fig. 5. Normalized line current spectra of the full-load PMSM in (a) healthy, (b) with 10% DE, (c) with 40% DE, and (d) experimental result for 50% DE case.

of the room. If this ball bearing is changed by the main ball bearing of the motor, there will a gap between the shaft and ball-bearing inner circumference and also between the outer circumference and ball-bearing room on the bung. These two

gaps can be filled by two rings with suitable dimensions. If these rings are eccentric, an ME generates in the motor. The smaller ring placed around the shaft generates DE, if the ring fixed on the shaft rotates with it. Other ring that is placed on the bung around the ball bearing creates SE. In this case, the rotor rotation axis coincides with its symmetrical axis but is displaced from the stator symmetrical axes. In this case, the distribution of the air gap around the rotor loses its uniformity, but it is time invariant. If these two eccentricities coexist, ME is created.

IV. SE, DE, AND ME FAULT DIAGNOSES

Following the calculation of the stator current using TSFEM, the determination of the stator current spectrum is necessary to introduce a frequency pattern. The maximum required frequency is around 150 Hz, and according to the Nyquist law, sampling frequency is set equal to 800 Hz. Meanwhile, the stator signal is considered over 4 s, which allows analyzing the signals with a frequency resolution of 0.25 Hz.

A. New Index for DE Fault Diagnosis

Fig. 5 shows the frequency spectrum of a healthy and faulty PMSM with 10% and 40% DE. A comparison between Fig. 5(a) and (b) illustrates that the 10% DE generates the sideband components at frequencies of 12.5, 37.5, 62.5, 87.5, 112.5, and 137.5 Hz. According to Fig. 5(b), the ASBCs of the aforementioned frequency are -89 , -103 , -108 , -99 , -100 , and -110 dB, respectively. Therefore, the generation of sideband components at the aforementioned frequencies and their amplitudes can be used to introduce a particular frequency pattern and a suitable index for the detection of DE fault. A comparison of Fig. 5(b) and (c) depicts that a 30% rise of the DE increases the ASBC at 12.5 Hz, from -89 to -83 dB. This is seen for frequencies 37.5, 62.5, 87.5, 112.5, and 137.5 Hz. According to Fig. 5(b) and (c), the ASBC at a frequency of 37.5 Hz increases from -103 to -96 dB, the ASBC at a frequency of 62.5 Hz increases from -108 to -98 dB, the ASBC at a frequency of 87.5 Hz increases from -99 to -97 dB, and the ASBC at a frequency of 112.5 Hz increases from -110 to -100 dB. Therefore, the comparison of Fig. 5(b) and (c) shows a considerable increase in the ASBC at the aforementioned frequencies. The ASBCs at these frequencies are shown in Table II for a healthy and faulty PMSM with 10%, 20%, 30%, and 40% DE. According to Fig. 5 and Table II, a DE degree rise increases the ASBC. Thus, a novel pattern frequency is introduced here, which enables one to diagnose the DE as follows:

$$f_{\text{Eccentricity}} = \left[1 \pm \left(\frac{2k-1}{P} \right) \right] f_s \quad (9)$$

where k is an integer number 1, 2, 3, \dots , P is the number of pole pairs, and f_s is the supply frequency. An interesting point in Fig. 5 and Table II is a considerable increase of ASBC at frequencies $[1 \pm (2k-1)/P]f_s$ due to DE fault and incremental rate due to higher DE degree.

TABLE II
COMPARISON OF CURRENT HARMONIC COMPONENTS
DUE TO DE, IN DECIBELS

Index: ASBC at	Dynamic Eccentricity Degree (%)				
	0	10	20	30	40
$(1-3/P)f_s$	---	-89	-87	-83	-76
$(1-1/P)f_s$	---	-103	-96	-91	-90
$(1+1/P)f_s$	---	-108	-102	-98	-93
$(1+3/P)f_s$	---	-99	-98	-97	-96
$(1+5/P)f_s$	---	-100	-97	-95	-91
$(1+7/P)f_s$	---	-110	-108	-100	-92

B. SE Fault Diagnosis

In the SE, the rotor rotation axis coincides with its symmetrical axis but is displaced to the stator symmetrical axis. In this case, the air gap surrounding the rotor will be nonuniform, but it is time independent. Due to the intrinsic tolerance in different parts of the motor and the method of mounting the parts, SE exists in different motors even in a new motor. The spectrum of the stator current of a healthy and faulty PMSM with 10% and 40% SE is shown in Fig. 6. A comparison of Figs. 5(a) and 6(a) indicates that the SE generates sideband components at frequencies $[1 \pm (2k - 1)/P]f_s$. Thus, the ASBC of the aforementioned pattern frequency can be used for the detection of SE. Meanwhile, a comparison of Fig. 6(a) and (b) shows that a higher degree SE increases the ASBC at frequencies $[1 \pm (2k - 1)/P]f_s$ considerably. It is noticeable that the incremental rate of the SE degree is sharper than that of the DE fault. Therefore, it is noticeable that the incremental rate of SE degree is sharper than that of the DE fault. Therefore, it is possible to discriminate the SE and DE faults using the difference between the ASBCs at $[1 \pm (2k - 1)/P]f_s$. The ASBCs at frequencies $[1 \pm (2k - 1)/P]f_s$ due to 0%, 10%, 20%, 30%, and 40% SE degrees are shown in Table III.

C. ME Fault Diagnosis

In this case, the symmetrical axis of the rotor and stator and the rotation axis of the rotor are displaced. The spectrum analysis of PMSM with 10% SE and 10% DE, and 30% SE and 40% DE is shown in Fig. 7. Referring to Fig. 7, the incremental rate of ASBC due to ME is more than that of the SE or DE case. To determine the portions of the SE and DE on the ASBC at frequencies $[1 \pm (2k - 1)/P]f_s$, the variation of ASBC at frequency $[1 - 1/P]f_s$ is shown versus the different degrees of SE and DE in Fig. 8. According to Fig. 8, the lowest ASBC at a frequency of $[1 - 1/P]f_s$ corresponds to the lowest SE and DE degrees. Meanwhile, the maximum ASBC at frequency $[1 - 1/P]f_s$ is in the maximum degree of the SE and DE. It is noted that the ASBC at the aforementioned frequency has been increased for a fixed degree of SE and the incremental degree of DE and also for a fixed degree of DE and the incremental degree of SE. However, the incremental rate of the ASBC at frequencies $[1 \pm (2k - 1)/P]f_s$ due to SE is more than that of the DE. Indeed, the effects of SE on the ASBC at frequencies of $[1 \pm (2k - 1)/P]f_s$ are more than that of the DE.

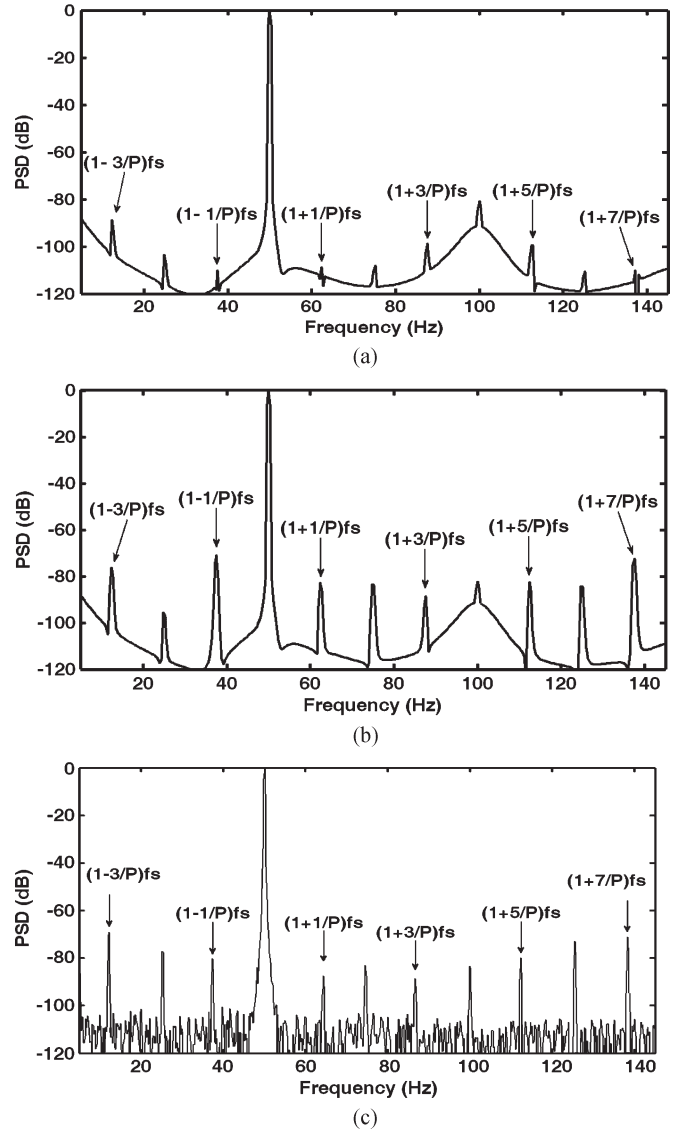


Fig. 6. Normalized line current spectra of the faulty full-load PMSM with (a) 10% SE, (b) 40% SE, and (c) experimental result for 50% SE case.

TABLE III
COMPARISON OF CURRENT HARMONIC COMPONENTS
DUE TO SE, IN DECIBELS

Index: ASBC at	Static Eccentricity Degree (%)				
	0	10	20	30	40
$(1-3/P)f_s$	---	-93	-82	-78	-71
$(1-1/P)f_s$	---	-85	-79	-72	-83
$(1+1/P)f_s$	---	-92	-88	-84	-81
$(1+3/P)f_s$	---	-97	-95	-93	-89
$(1+5/P)f_s$	---	-100	-93	-87	-82
$(1+7/P)f_s$	---	-87	-82	-75	-72

V. LOAD EFFECTS ON THE PROPOSED INDEX

One of the most important problems in any fault diagnosis method is the investigation of load variation on the proposed indices. Accurate fault detection is not possible without definition of relations between indices, load variations, and eccentricity percentages. In [22], the effects of load variation on the global indices have been analyzed for eccentricity fault diagnosis

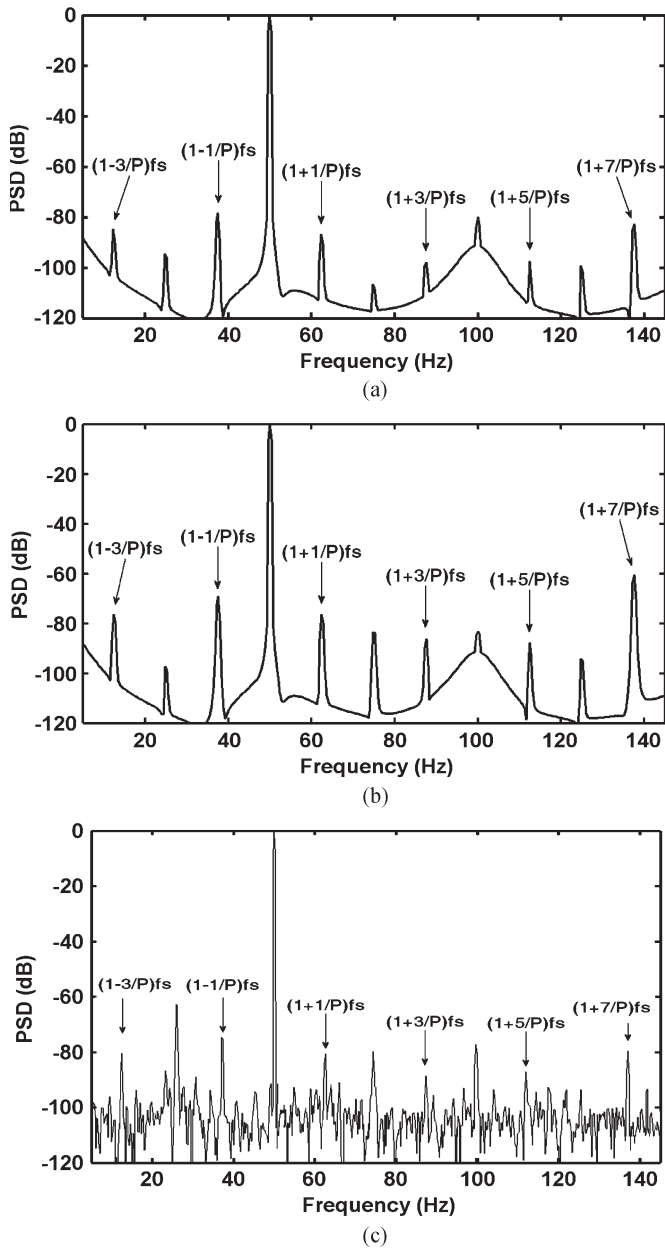


Fig. 7. Normalized line current spectra of the faulty full-load PMSM with (a) 10% SE and 10% DE, (b) 30% SE and 40% DE, and (c) experimental result for 10% SE and 10% DE.

in induction motors. It has been shown that load increases cause the ASBC to decrease at frequencies $(f_s \pm k f_r)$, which has been utilized for eccentricity fault diagnosis in induction motors. Meanwhile, it has been emphasized that precise fault detection depends on the comparison of healthy and faulty induction motors in the same loads. The reason is the close relation between the slip as a parameter which expresses load variation and the aforementioned indices (ASBC at $f_s \pm k f_r$). In [23], the impacts of load variation have been studied on broken bar fault diagnosis in induction motors. It has been illustrated that ASBC at frequencies $(1 \pm 2ks) f_s$ rises due to the load increases. It is also necessary to compare healthy and faulty induction motor with broken bars in the same loads to accurate fault detection.

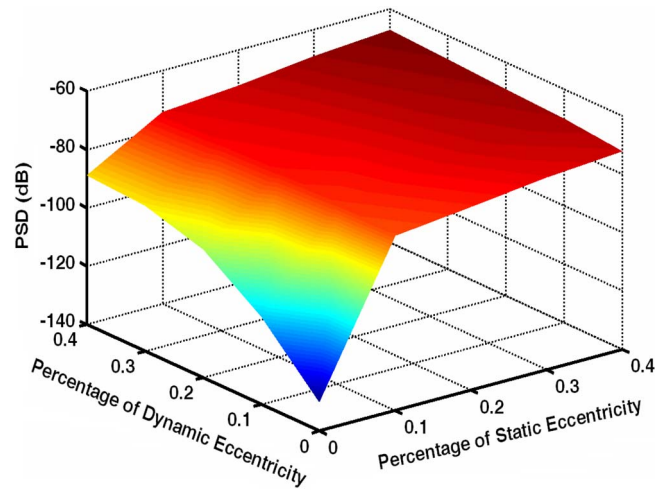


Fig. 8. Amplitude variation of sideband component versus SE and DE degrees at a frequency of $[1 - 1/P] f_s$ (37.5 Hz).

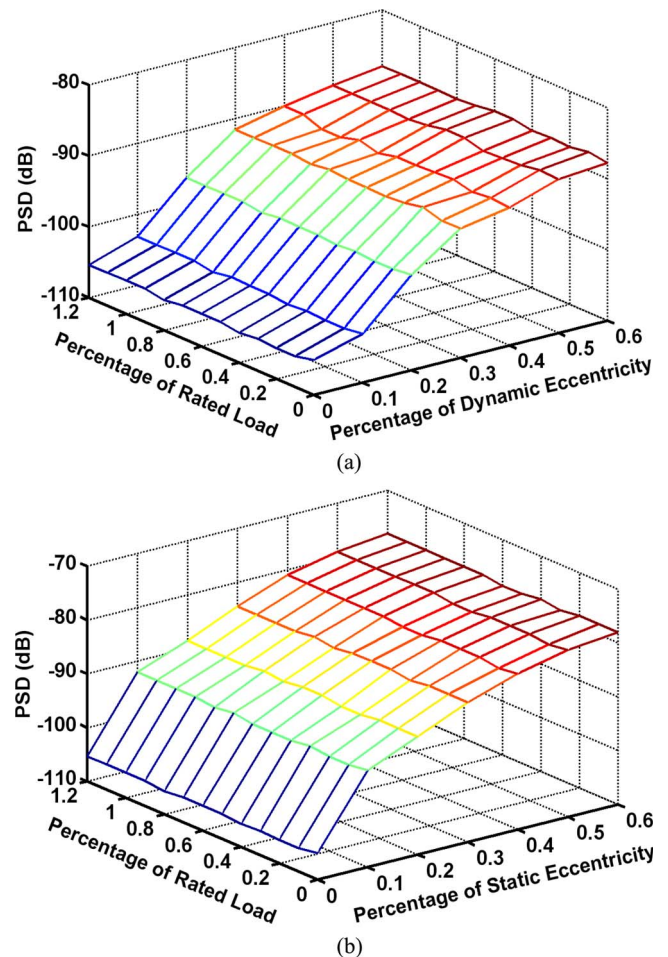


Fig. 9. Amplitude variation of sideband component versus load variation and different percentages of (a) DE and (b) SE.

The variation of ASBC at frequency $(1 - 1/P) f_s$ is shown versus different DE percentages and load levels in Fig. 9(a). Since motor speed is constant at synchronous speed in PMSMs, load variations do not have noticeable impacts on the ASBC at the same eccentricity percentage. According to Fig. 9(a), the ASBC at frequency $(1 - 1/P) f_s$ rises due to increases

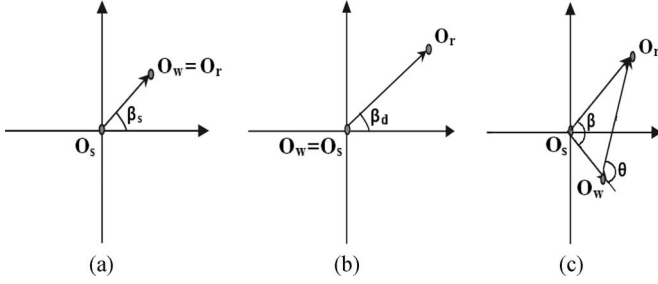


Fig. 10. Position of stator and rotor cross sections under (a) SE, (b) DE, and (c) ME in the stator reference frame.

of eccentricity percentage, and it is fairly constant for load variation from 0% to 120% rated load. Indeed, the proposed index in this paper is robust against load variation, and it is not necessary to specify motor load for accurate fault detection. Therefore, this index is much more efficient than global indices which are utilized for eccentricity fault diagnosis in induction motors. Fig. 9(b) shows the load variation of ASBC at frequency $(1 + 1/P)f_s$ for different SE percentages and load levels. Fig. 9(b) shows that, albeit the introduced index does not change perceptibility due to load variations, it increases considerably due to the SE fault occurrence and its percentage increases. A comparison between Fig. 9(a) and (b) demonstrates same behavior from the proposed index against load variation. Meanwhile, it represents that the sensitivity of the introduced index for the SE is more than the DE fault.

VI. THEORETICAL ANALYSIS OF THE INTRODUCED INDEX

Magnetic field contains full information about the stator, rotor, and mechanical parts of the motor. Thus, continuous monitoring of the air-gap magnetic field can be employed to detect all faults in electrical machines. To analyze the magnetic flux density of the air gap, the computation of air-gap permeance in the faulty motor is necessary.

A. Air-Gap Permeance

In the SE fault, the rotational axis of the rotor coincides with the rotor symmetrical axis, and it is displaced from the stator symmetrical axis. Although the air-gap distribution around the rotor is not uniform, it is time independent. The SE degree (δ_s) is defined as follows:

$$\delta_s = \frac{|O_s O_w|}{g} \quad (10)$$

where O_s is the stator symmetry center, O_w is the rotor rotation center, and g is the uniform air-gap length. Fig. 10(a) shows the position of stator and rotor cross sections in the SE, where β_s is the initial angle of the SE and vector $O_s O_w$ is the static transfer vector. This vector is fixed for all angular positions of the rotor.

In the DE fault, the minimum air-gap length depends on the rotor angular position, and it rotates around the rotor. In this eccentricity, the symmetry axis of the stator and the rotation axis of the rotor are identical, but the rotor symmetry axis has been displaced. In such a case, the air gap around the rotor is

nonuniform and time varying. The DE degree (δ_d) is defined as follows:

$$\delta_d = \frac{|O_w O_r|}{g} \quad (11)$$

where O_r is the rotor symmetrical axis, and vector $O_w O_r$ is the dynamic transfer vector. This vector is fixed for all angular positions of the rotor, but its angle varies. Fig. 10(b) shows the DE, where β_d is the initial angle of the DE. In the ME fault, the symmetry axis of the rotor and stator and the rotation axis of the rotor are displaced. This is the result of the application of the resultant vector of static and dynamic transfer vectors. If there are both SE and DE, the symmetry axis of the rotor and stator and the rotation axis of the rotor are displaced. This is the result of the application of the resultant vector of the static and dynamic transfer vectors. If there are both SE and DE, the eccentricity is called an ME. The ME degree (δ_m) is defined as follows:

$$\delta_m = \frac{|O_s O_r|}{g} = \left| \frac{O_s O_w}{g} + \frac{O_w O_r}{g} \right| = \sqrt{\delta_s^2 + \delta_d^2 + 2\delta_s \delta_d \cos \theta}$$

$$\beta = \angle O_s O_r = \tan^{-1} \frac{\delta_d \sin \theta}{\delta_s + \delta_d \cos \theta} \quad (12)$$

where vector $O_s O_r$ is the mixed transfer vector. Fig. 10(c) shows that the amplitude and angle of this vector depend on the mechanical angle of the rotor, where β is the transfer angle of the ME. Thus, the air-gap length in the faulty PMSM under ME depends on the rotor mechanical angle and is defined as follows:

$$g(t) = R_s - \delta_m g \cos \left(\frac{\omega t}{P} - \beta \right) - \sqrt{R_r^2 - \delta_m^2 g^2 \sin^2 \left(\frac{\omega t}{P} - \beta \right)} \quad (13)$$

where $g(t)$ is the air-gap length in the faulty PMSM under ME, R_s is the stator radius, ω is the supply frequency, and R_r is the rotor radius. Meanwhile, the average of air-gap length is as follows:

$$r_{av}(t) = R_s - 0.5g(t). \quad (14)$$

Since the air-gap permeance is the inversion of magnetic reluctance, it can be determined as follows:

$$H(t) = \mu_0 \frac{r_{av}(t)}{g(t)} = \mu_0 \frac{0.5R_s + 0.5\delta g \cos(\frac{\omega t}{P} - \beta) + 0.5\sqrt{R_r^2 - \delta_m^2 g^2 \sin^2(\frac{\omega t}{P} - \beta)}}{R_s - \delta g \cos(\frac{\omega t}{P} - \beta) - \sqrt{R_r^2 - \delta_m^2 g^2 \sin^2(\frac{\omega t}{P} - \beta)}} \quad (15)$$

where μ_0 is the permeability of free space. It is noticeable that the air-gap length is much lesser than the rotor radius, and thus, it is assumed that

$$\sqrt{R_r^2 - \delta_m^2 g^2 \sin^2 \left(\frac{\omega t}{P} - \beta \right)} \cong R_r. \quad (16)$$

Therefore, (15) can be rewritten as follows:

$$H(t) = \mu_0 \frac{0.5(R_s + R_r)}{(R_s - R_r) - \delta_m g \cos\left(\frac{\omega t}{P} - \beta\right)}. \quad (17)$$

However, $R_s - R_r = g$, and (17) can be simplified as follows:

$$H(t) = \frac{0.5\mu_0}{g} \frac{(R_s + R_r)}{(1 - \delta_m \cos\left(\frac{\omega t}{P} - \beta\right))}. \quad (18)$$

It is assumed that $0.5\mu_0(R_s + R_r)/g = h_0$; the air-gap permeance is expressed as follows:

$$H(t) = \frac{h_0}{1 - \delta_m \cos\left(\frac{\omega t}{P} - \beta\right)}. \quad (19)$$

Equation (19) can be presented as a Fourier series as follows:

$$H(t) = \frac{2h_0}{\sqrt{1 - \delta_m^2}} + \frac{2h_0}{\sqrt{1 - \delta_m^2}} \times \sum_{k=1}^{\infty} \left\{ \left(\frac{1 - \sqrt{1 - \delta_m^2}}{\delta_m} \right)^k \cos k \left(\frac{\omega t}{P} - \beta \right) \right\}. \quad (20)$$

It is obvious that the air-gap permeance of SE or DE is evaluated only by inserting $\delta_s = 0$ or $\delta_d = 0$ in (20), respectively.

B. Air-Gap Field Components

Since one stator electrical fundamental period produces only $1/P$, a rotation for a P pole pairs machine, and the position of minimum air gap rotates with the rotor, the flux linkage, magnetic flux density, and winding inductances will be different in $1/P$ of the rotation compared to other $(P - 1)/P$ of rotation. By applying the Ampere's circuital law, the stator air-gap field can be computed as follows:

$$B_s(\phi, t) = H(t) \int \mu_0 j_s(\phi, t) d\phi \quad (21)$$

where $j_s(\phi, t)$ is the current density on the stator inner surface and can be expressed as follows:

$$j_s(\phi, t) = J_s \sin(\omega t - \phi) \quad (22)$$

where J_s is the peak of the peak of the current density. Therefore, magnetic flux density can be written by combining (20)–(22) as follows:

$$B_s(\varphi, t) = \left(\frac{h_0}{\sqrt{1 - \delta_m^2}} + \frac{2h_0}{\sqrt{1 - \delta_m^2}} \times \sum_{k=0}^{\infty} \left\{ \left(\frac{1 - \sqrt{1 - \delta_m^2}}{\delta_m} \right)^k \cos k \left(\frac{\omega t}{P} - \beta \right) \right\} \right) \times \int \mu_0 J_s \sin(\omega t - \varphi) d\varphi. \quad (23)$$

Equation (23) can be rewritten as follows:

$$B_s(\varphi, t) = \left(\frac{h_0}{\sqrt{1 - \delta_m^2}} + \frac{2h_0}{\sqrt{1 - \delta_m^2}} \times \sum_{k=0}^{\infty} \left\{ \left(\frac{1 - \sqrt{1 - \delta_m^2}}{\delta_m} \right)^k \cos k \left(\frac{\omega t}{P} - \beta \right) \right\} \right) \times (\mu_0 J_s \cos(\omega t - \varphi)). \quad (24)$$

Equation (24) can be derived as follows:

$$B_s(\varphi, t) = \frac{\mu_0 h_0 J_s}{\sqrt{1 - \delta_m^2}} \cos(\omega t - \varphi) + \frac{2\mu_0 h_0 J_s}{\sqrt{1 - \delta_m^2}} \times \sum_{k=0}^{\infty} \left\{ \left(\frac{1 - \sqrt{1 - \delta_m^2}}{\delta_m} \right)^k \cos k \left(\frac{\omega t}{P} - \beta \right) \cos(\omega t - \varphi) \right\}. \quad (25)$$

By multiplying the cosine statements in the parentheses (25) can be simplified as follows:

$$B_s(\varphi, t) = \frac{\mu_0 h_0 J_s}{\sqrt{1 - \delta_m^2}} \cos(\omega t - \varphi) + \frac{\mu_0 h_0 J_s}{\sqrt{1 - \delta_m^2}} \times \left\{ \sum_{k=0}^{\infty} \left(\frac{1 - \sqrt{1 - \delta_m^2}}{\delta_m} \right)^k \times \left[\text{Cos} \left(\left(1 - \frac{k}{P} \right) \omega t + \beta - \varphi \right) + \text{Cos} \left(\left(1 + \frac{k}{P} \right) \omega t - \beta - \varphi \right) \right] \right\}. \quad (26)$$

To determine an expression for the rotor MMF wave components, it is assumed that $\varphi = \omega t + \varphi'$ and a similar scrutiny can be carried out for rotor air-gap field. Therefore, the air-gap field can be written as follows:

$$B(t) = B_0 \cos(\omega t - \varphi_0) + \left\{ \sum_{k=0}^{\infty} B_k \left[\text{Cos} \left(\left(1 - \frac{k}{P} \right) \omega t - \varphi_1 \right) + \text{Cos} \left(\left(1 + \frac{k}{P} \right) \omega t - \varphi_2 \right) \right] \right\}. \quad (27)$$

C. Stator Current Components

The impacts of eccentricity on the current spectrum can be determined by the analysis of the corresponding magnetic flux density components. Hence, MMF considering eccentricity fault can be defined as follows:

$$F(t) = B(t)g(t). \quad (28)$$

The stator current is determined by combining (13), (16), and (27) as follows:

$$i(t) = I_0 \cos(\omega t - \psi) + \left\{ \sum_{k=0}^{\infty} I_k \left[\text{Cos} \left(\left(1 - \frac{k}{P} \right) \omega t - \Phi \right) + \text{Cos} \left(\left(1 + \frac{k}{P} \right) \omega t - \Omega \right) \right] \right\}. \quad (29)$$

According to (29), sideband components at frequencies $(1 \pm k/P)f_s$ ($k = 1, 2, 3, \dots$) are observed in the distribution of magnetic flux density of the faulty motor. Thus, $(1 \pm k/P)f_s$ as a frequency pattern and the ASBC at frequencies $(1 \pm k/P)f_s$ can be utilized as a proper index for eccentricity fault diagnosis in PMSMs. Since the main field generates harmonic components at frequencies 50 Hz ($k = 0$), 100 Hz ($k = 4$), 150 Hz ($k = 8$), 200 Hz ($k = 12$), ..., etc., due to the associated rotating force wave, and also the magnitude of these harmonic components is more dominant than the magnitude of the aforementioned harmonic components due to eccentricity, the amplitude of harmonic components at frequencies 50, 100 Hz, ..., due to eccentricity is negligible. Thus, it is not possible to recommend a frequency pattern which is based on the even coefficients ($k = 2, 4, 6, 8, \dots$). Therefore, the ASBCs at odd coefficients ($k = 1, 3, 5, \dots$), in which some of them are expressed as follows, are introduced as a proper and efficient index:

$$\begin{aligned}
 i(t) = & I_1 \text{Cos} \left(\left(1 - \frac{3}{P} \right) \omega t - \Phi \right) + I_2 \text{Cos} \left(\left(1 - \frac{1}{P} \right) \omega t - \Phi \right) \\
 & + I_3 \text{Cos} \left(\left(1 + \frac{1}{P} \right) \omega t + \Omega \right) + I_4 \text{Cos} \left(\left(1 + \frac{3}{P} \right) \omega t + \Omega \right) \\
 & + I_5 \text{Cos} \left(\left(1 + \frac{5}{P} \right) \omega t + \Omega \right) + I_6 \text{Cos} \left(\left(1 + \frac{7}{P} \right) \omega t + \Omega \right)
 \end{aligned} \tag{30}$$

where I_1, \dots, I_6 are coefficients which are calculated from (26). Referring to Figs. 5–7 illustrates this fact obviously.

VII. ANALYSIS OF THE PROPOSED INDICES FOR ESTIMATING THE TYPE AND DEGREE OF ECCENTRICITY

The proposed indices are employed for the detection and severity estimation of both pure SE and DE. To estimate the eccentricity degree, first, its type must be identified, and then, the degree must be estimated. Thus, a hierarchical scheme can be employed for classification. The first classifier only decides whether the eccentricity is purely static or dynamic, and then, another classifier estimates the severity of eccentricity according to its type. To evaluate the ability of the proposed index for eccentricity detection and estimation of its severity, first, the correlation between index and eccentricity degree is calculated (Table IV). Then, a k -NN classifier is employed for the diagnosis of the eccentricity type, and then, three-layer ANNs are employed to classify the current profile. As a good index, it needs to have high recognition rate along with robust performance to environmental changes, i.e., the index must have low sensitivity to the parameter changes. The most important parameter in these tasks is noise measurement. To evaluate the robustness of the proposed indices, white Gaussian noise is added to the simulated current, and the variance of the noise is gradually increased until the recognition rate become unacceptable. It seems that the proposed indices are capable to discriminate different eccentricities.

TABLE IV
CORRELATION COEFFICIENT BETWEEN THE PROPOSED INDICES AND ECCENTRICITY DEGREES. (UPPER ROW) ρ VERSUS SE. (LOWER ROW) ρ VERSUS DE

S/N	$[1-3/p]f_s$	$[1-1/p]f_s$	$[1+1/p]f_s$	$[1+3/p]f_s$	$[1+5/p]f_s$	$[1+7/p]f_s$
Noise	0.9213	0.9392	0.9488	0.9531	0.9642	0.9423
60 dB	0.877	0.635	0.921	0.973	0.935	0.536
50 dB	0.9174	0.9381	0.941	0.948	0.9504	0.924
40 dB	0.873	0.629	0.917	0.957	0.931	0.532
30 dB	0.9477	0.9537	0.9351	0.8038	0.9282	0.9529
20 dB	0.825	0.601	0.902	0.862	0.927	0.488
Noise	0.8464	0.8252	0.6365	0.5192	0.6222	0.8466
60 dB	0.663	0.442	0.411	0.458	0.731	0.431
50 dB	0.5845	0.5029	0.242	0.3581	0.3606	0.5215
40 dB	0.412	0.327	0.221	0.287	0.426	0.243
30 dB	0.33	0.2675	0.0666	0.164	0.0376	0.2429
20 dB	0.27	0.17	0.093	0.043	0.112	0.038

TABLE V
ESTIMATION OF ECCENTRICITY TYPE BY THE PROPOSED INDICES

Signal to noise ratio	Correct Classification Rate
No noise	100
60dB	100
50dB	100
40dB	99.38
30dB	97.06
20dB	92.71

VIII. ECCENTRICITY SEVERITY ESTIMATION

To estimate the eccentricity severity, first, its type must be identified, and then, its severity is estimated. For better analysis of the results, a k -NN classifier is employed for identifying the eccentricity type, and MLP neural networks are used to estimate eccentricity severity.

A. Identifying Eccentricity Type

The fault detection procedure can be divided into two phases. At the first phase, its type must be identified. k -NNs are a nonparametric classifier based on nonparametric estimation of the class densities. k -NN classifiers find k -nearest samples in some reference set, by taking a majority vote among the classes of these k samples. It turns out that it is the estimation of the posterior probability by the proportions of the classes among the k samples. The aim is to find the NNs of an undefined test pattern within a hypersphere of a predefined radius in order to determine its true class. Various distance measures can be used, including the Euclidean and Mahalanobis distance. The simplest version of the algorithm is for $k = 1$, known as the NN rule. In other words, a feature vector x is assigned to the class of its NN. Provided that the number of training samples is large enough, this simple rule exhibits a good performance. A single NN method ($k = 1$) is primarily suited to recognizing data where one has sufficient confidence in the fact that class distributions are nonoverlapping and the features used are discriminatory. In most practical applications, however, the data distributions for various classes are overlapping, and more than one NN is used for majority voting. As this classifier is well known for two class problems in electrical machine fault detection (healthy or faulty machine) [20] with impressive

TABLE VI
ANN CLASSIFICATION RESULTS FOR ECCENTRICITY DEGREE ESTIMATION. (GRAY) SE. (WHITE) DE

Signal to noise ratio (S/N)	Number of neurons in the hidden layer	Average of correct Classification results on training set (%)	Average of correct Classification results on test set (%)	Standard deviation of classification results on train set over 20 experiments (%)	Standard deviation of classification results on test set over 20 experiments (%)	Best classification result on test set (%)	Worst classification results on test set (%)
No noise	6	100	99.2	0.95	1.21	100	95.33
	7	100	99.31	0.89	1.14	100	95.94
60 dB	7	100	99.03	1.01	1.29	100	95.1
	7	100	98.21	1.18	1.42	100	94.7
50 dB	9	99.35	98.1	1.05	1.34	99.9	94.1
	8	98.9	97.53	1.34	2.46	99.3	91.4
40 dB	10	98.8	95.6	1.1	1.88	98.76	90.24
	9	96.32	93.21	1.57	2.86	96.24	87.3
30 dB	13	97.27	90.5	1.13	2.10	95.0	86.67
	15	91.62	86.27	2.15	2.96	90.2	80.13
20 dB	15	93.24	83.7	2.67	4.22	91.1	75.39
	16	88.91	78.68	3.24	5.96	85.22	63.77

results, here, it is employed for estimating the eccentricity type. The result of classification by current indices with various noise variances is presented in Table V, in which the proposed indices can completely distinct two types of eccentricity. As the noise level is increased, their ability decreased, but even at $S/N = 20$ dB, the correct classification rate is acceptable.

B. Estimation of Eccentricity Degree

The main objective in fault detection system is the estimation of fault severity; thus, the ability of these indices must be evaluated by using a classification system. Therefore, a multilayer perceptron ANN is utilized for the estimation of eccentricity severity. The utilization of ANNs for pattern classification has been deeply studied [21]. Here, it is assumed that the eccentricity type is detected correctly, and we want to evaluate their ability for the estimation of eccentricity degree in the case of pure SE or DE.

C. Architecture of Networks

A three-layer feedforward perceptron ANN trained by a back-propagation learning rule was used for the classification. To evaluate the separability of classes with different combinations of features, different architectures were utilized. The number of output nodes was fixed to the number of classes of SEs (or DEs), and the number of input nodes was set equal to the dimension of feature vector. The number of neurons in the hidden layer was the parameter used for the optimization of the structure of the network. The number of neurons in the hidden layer is usually selected based on the dimension of the feature vector and the level of the complication of relationships between classes.

D. Results

In this part, the indices extracted from the motor current are classified. As the data set consists of 100 current vectors for

each pure SE and DE degrees, 280 feature vectors are used as the training set (about 70% of the total data) randomly, and the others are employed to test the classification performance. The reported results are acquired using 20 rounds of training–testing experiments on the optimum network. The classification results for SE estimation are presented in Table VI, including the number of neurons in the hidden layer, average success of the network on the training, and test sets. The standard deviation, and the best and worst performances of the classification results are also reported in the table. It is clear that both indices are able to classify different types and degrees of eccentricities with small error in both test and train sets. Due to high capability for eccentricity classification, the proposed indices can be used to develop high-performance fault detection systems. As we expected from the correlation analysis, noise has more effect on the DE estimation, and the performance of the classification degrades significantly in the presence of high noise.

IX. DISCRIMINATION BETWEEN ECCENTRICITY AND OTHER FAULTS USING THE INTRODUCED INDEX

One of the most important characteristics which the introduced index should have is being perceptive against eccentricity fault occurrence and its expansion and also being robust against other faults. In this case, it is claimed that the proposed index is a proper criterion to detect that fault. According to Fig. 1, magnetic and electrical faults might happened in PMSMs, and thus, the current spectrum of the faulty PMSM under the aforementioned faults should be investigated. Indeed, the ability of magnetic fault (PM demagnetization) and electrical faults (short and open circuits) to generate sideband components at frequencies $[1 \pm (2k - 1)/P]f_s$ in the current spectrum should be defined. For this, the current spectrum of the PMSM under short circuit, open circuit, and PM demagnetization around fundamental harmonic (5–145 Hz) is analyzed to compare with eccentricity fault.

Fig. 11 shows the current spectrum of the faulty PMSM under one-phase short circuit, one-phase open circuit, and one

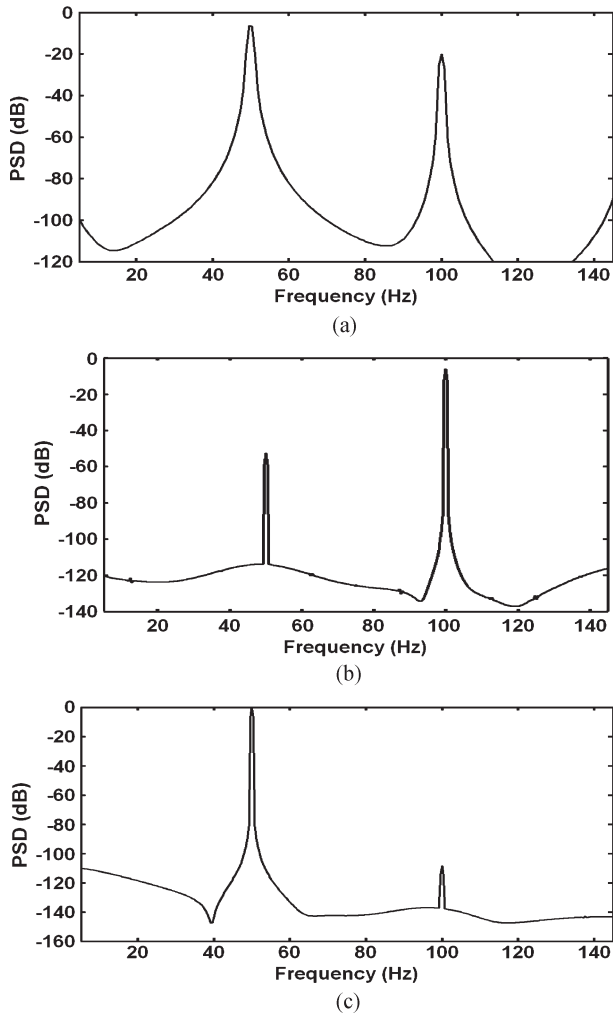


Fig. 11. Normalized line current spectra of the faulty full-load PMSM with (a) short circuit, (b) open circuit, and (c) demagnetization of one PM.

PM demagnetization. Fig. 11 shows that sideband components at frequencies $[1 \pm (2k - 1)/P]f_s$ are not generated due to magnetic and electrical faults. Therefore, the frequency pattern which is introduced for eccentricity fault diagnosis in PMSMs is unique, and aforementioned faults do not generate these components. Meanwhile, using this index makes the discrimination between eccentricity fault and other faults easy, which can be utilized to predict fault type as magnetic, electrical, and mechanical faults.

One of the most important points in Fig. 11(a) and (b) is that the current spectrum is normalized but the peaks of amplitudes seem to be around -5 dB, whereas the maximum magnitude of the current spectrum due to eccentricity fault relates fundamental harmonic (50 Hz), which is shown in Figs. 5–7. This is due to dc component at 0 Hz in the current spectrum of the PMSM under electrical faults, which has the maximum amplitude in Fig. 11(a) and (b). It is noticeable that, for having a good resolution and a proper presentation of sideband components due to faults, the dc component has been ignored using the demonstration of sideband components after 5 Hz in Figs. 5–7 and Fig. 11. Albeit magnetic and electrical faults do not create sideband components at frequencies $[1 \pm (2k -$

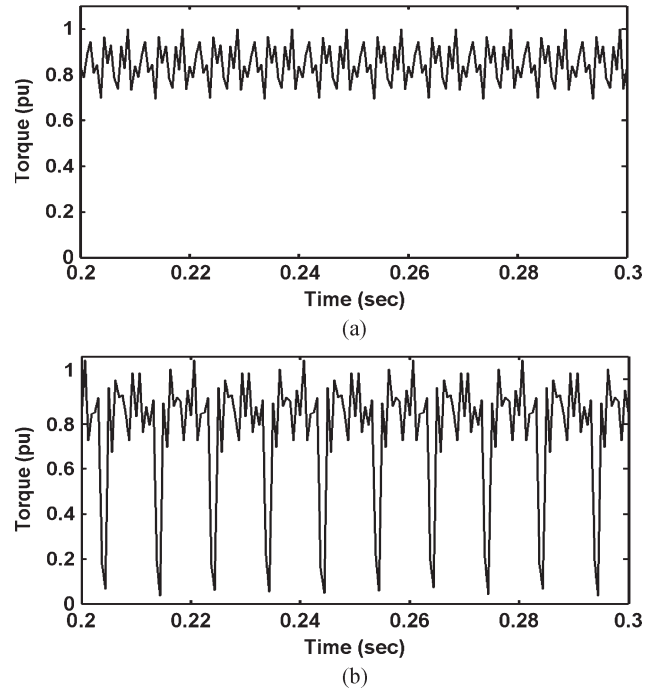


Fig. 12. Time variation of the developed torque in (a) healthy and (b) faulty motors with demagnetization of one PM.

$1)/P]f_s$ at the current spectrum, these faults disturb PMSM performance, which is too harmful for motor efficiency and its lifetime. Fig. 12 shows the developed torque in the healthy and faulty motors with demagnetized PM. Fig. 12 shows that demagnetization disturbs motor performance considerably.

X. CONCLUSION

This paper has indicated how the SE, DE, and ME of PMSM can be diagnosed. A novel pattern frequency has been introduced for the diagnosis of eccentricity and the determination of its type and degree. A model of the faulty PMSM with SE, DE, and ME using TSFEM was shown. The spectrum of stator current was calculated using FFT, and the amplitude of this pattern was introduced as a proper index. The proposed index was robust against load variation, and it is not necessary to specify motor load for accurate fault diagnosis. Thus, this index is much more efficient than global indices which are employed for eccentricity fault diagnosis in induction motors. Meanwhile, a comparison between the spectrum current of the faulty PMSM due to eccentricity and open circuit, short circuit, and demagnetization illustrates that only eccentricity generates these kinds of sideband components. Thus, discrimination between eccentricity and other faults using this index is possible. To evaluate the effectiveness of the proposed index, correlation analysis was performed. The eccentricity type was then determined by a k -NN classifier, and three-layer ANNs were employed to estimate the eccentricity degree. White Gaussian noise was added to the simulated current, and the robustness of the proposed index was analyzed with respect to the noise variance. The proposed index could estimate the value of eccentricity and its type with acceptable error rate, and it can be used for developing highly accurate fault detection system for PMSMs.

REFERENCES

- [1] M. S. K. Khan and M. A. Rahman, "Development and implementation of a novel fault diagnostic and protection technique for IPM motor drives," *IEEE Trans. Ind. Electron.*, vol. 56, no. 1, pp. 85–92, Jan. 2009.
- [2] E. G. Strangas, S. Aviyente, and S. S. H. Zaidi, "Time-frequency analysis for efficient fault diagnosis and failure prognosis for interior permanent-magnet AC motors," *IEEE Trans. Ind. Electron.*, vol. 55, no. 12, pp. 4191–4199, Dec. 2008.
- [3] Z. Sun, J. Wang, D. Howe, and G. Jewell, "Analytical prediction of short-circuit current in fault-tolerant permanent magnet machines," *IEEE Trans. Ind. Electron.*, to be published, DOI: 10.1109/TIE.2008.2003210.
- [4] M. M. Blodt, P. P. Granj, B. B. Raison, and G. G. Rostaing, "Models for bearing damage detection in induction motors using stator current monitoring," *IEEE Trans. Ind. Electron.*, vol. 55, no. 4, pp. 1813–1822, Apr. 2008.
- [5] B. Akin, U. Orguner, H. A. Toliyat, and M. Rayner, "Low order PWM inverter harmonics contributions to the inverter-fed induction machine fault diagnosis," *IEEE Trans. Ind. Electron.*, vol. 55, no. 2, pp. 610–619, Feb. 2008.
- [6] M. Blodt, D. Bonacci, J. Regnier, M. Chabert, and J. Faucher, "On-line monitoring of mechanical faults in variable-speed induction motor drives using the Wigner distribution," *IEEE Trans. Ind. Electron.*, vol. 55, no. 2, pp. 522–533, Feb. 2008.
- [7] R. N. Andriamalala, H. Razik, L. Baghli, and F. Sargos, "Eccentricity fault diagnosis of a dual-stator winding induction machine drive considering the slotting effects," *IEEE Trans. Ind. Electron.*, vol. 55, no. 12, pp. 4238–4251, Dec. 2008. DOI: 10.1109/TIE.2008.2004664.
- [8] U. Kim and K. Lieu, "Magnetic field calculation in permanent magnet motors with rotor eccentricity: Without slotting effect," *IEEE Trans. Magn.*, vol. 34, no. 4, pp. 2243–2252, Jul. 1998.
- [9] U. Kim and K. Lieu, "Magnetic field calculation in permanent magnet motors with rotor eccentricity: With slotting effect considered," *IEEE Trans. Magn.*, vol. 34, no. 4, pp. 2253–2266, Jul. 1998.
- [10] T. J. Kim, S. M. Hwang, K. T. Kim, W. B. Jung, and C. U. Kim, "Comparison of dynamic responses for IPM and SPM motors by considering mechanical and magnetic coupling," *IEEE Trans. Magn.*, vol. 37, no. 4, pp. 2818–2820, Jul. 2001.
- [11] L. S. Stephens and M. A. Casemore, "Influence of stator slot geometry and rotor eccentricity on field distribution in cylindrical magnetic actuators," *IEEE Trans. Magn.*, vol. 38, no. 2, pp. 1348–1356, Mar. 2002.
- [12] J. P. Wang and K. Lieu, "Magnetic lumped parameter modeling of rotor eccentricity in brushless permanent magnet motors," *IEEE Trans. Magn.*, vol. 35, no. 5, pp. 4226–4231, Sep. 1999.
- [13] J. Gieras, "Analytical approach to cogging torque calculation of PM brushless motors," *IEEE Trans. Ind. Appl.*, vol. 40, no. 5, pp. 1310–1316, Sep. 2004.
- [14] T. Yoon, "Magnetically induced vibration in a permanent magnet brushless DC motor with symmetric pole-slot configuration," *IEEE Trans. Magn.*, vol. 41, no. 6, pp. 2173–2179, Jun. 2005.
- [15] M. Rosu, J. Saitz, and A. Arkkio, "Hysteresis model for finite element analysis of permanent magnet demagnetization in a large synchronous motor under a fault condition," *IEEE Trans. Magn.*, vol. 41, no. 6, pp. 2118–2123, Jun. 2005.
- [16] A. R. C. Sekhar Babu, K. R. Rajagopal, and P. R. Upadhyay, "Performance prediction of multiphase doubly salient permanent magnet motor having non-uniform air gap," *IEEE Trans. Magn.*, vol. 42, no. 10, pp. 3503–3505, Oct. 2006.
- [17] W. L. Roux, R. G. Harley, and T. G. Habetler, "Detection rotor faults in low power permanent magnet synchronous machines," *IEEE Trans. Power Electron.*, vol. 22, no. 1, pp. 322–328, Jan. 2007.
- [18] C. C. Hawang, C. M. Chang, C. K. Chan, C. T. Pan, and T. Y. Chang, "Comparison of performances between IPM and SPM motors with rotor eccentricity," *J. Magn. Magn. Mater.*, vol. 282, pp. 360–363, May 2004.
- [19] A. M. Trzynadlosky, "Diagnostic of mechanical abnormalities in induction motor using instantaneous electric power," in *Proc. Int. Elect. Mach. Drives Conf.*, Milwaukee, WI, 1997, pp. 91–93.
- [20] R. O. Duda, P. E. Hart, and D. G. Stork, *Pattern Classification*, 2nd ed. New York: Wiley, 2002.
- [21] G. Niu, J. D. Son, A. Widodo, B. S. Yang, D. H. Hwang, and D. S. Kang, "A comparison of classifier performance for fault diagnosis of induction motor using multi-type signals," *Struct. Health Monit.*, vol. 6, no. 3, pp. 215–229, 2007.
- [22] J. Faiz, B. M. Ebrahimi, B. Akin, and H. A. Toliyat, "Comprehensive eccentricity fault diagnosis in induction motors using finite element," *IEEE Trans. Magn.*, vol. 45, no. 3, pp. 1764–1767, Mar. 2009.
- [23] A. Bellini, F. Filippetti, G. Francheschini, C. Tassoni, R. Passaglia, M. Saottini, G. Tontini, M. Giovannini, and A. Rossi, "Quantitative evaluation of induction motor broken bars by means of electrical signature analysis," *IEEE Trans. Ind. Appl.*, vol. 37, no. 5, pp. 1248–1255, Sep./Oct. 2001.



Bashir Mahdi Ebrahimi was born in Iran in 1979. He received the B.Sc. and M.Sc. (with honors) degrees from the University of Tabriz, Tabriz, Iran, in 2004 and 2006, respectively. He is currently working toward the Ph.D. degree in electrical engineering in the School of Electrical and Computer Engineering, University of Tehran, Tehran, Iran.

He was a Top Student Researcher with the University of Tehran in 2008. He has published 27 papers in journals and 25 papers in international conference proceedings. His research interests include design,

modeling, control, and fault diagnosis of electrical machines, and finite-element analysis of electromagnetic devices.



Jawad Faiz (M'90–SM'93) received the Ph.D. degree in electrical engineering from the University of Newcastle-upon-Tyne, Newcastle-upon-Tyne, U.K., in 1988.

He is currently a Professor in the School of Electrical and Computer Engineering, University of Tehran, Tehran, Iran. His teaching and research interests are switched reluctance and variable reluctance motor design, and the design and modeling of electrical machines and drives.

Dr. Faiz is a member of the Iran Academy of

Science.



Mehryan Javan Roshtkhari was born in Mashhad, Iran, in 1984. He received the B.Sc. and M.Sc. degrees in electrical engineering from the University of Tehran, Tehran, Iran, in 2006 and 2009, respectively. He is currently working toward the Ph.D. degree in electrical engineering at McGill University, Montreal, QC, Canada.

His research interests include pattern recognition, signal processing, and electrical machine fault diagnosis.